Spectrochimica Acta Part A: Molecular and Biomolecular Spectroscopy 97 (2012) 202–208

Contents lists available at SciVerse ScienceDirect

Spectrochimica Acta Part A: Molecular and Biomolecular Spectroscopy

journal homepage: www.elsevier.com/locate/saa

Structural study, coordinated normal analysis and vibrational spectra of 4-hydroxy-3-(3-methyl-2-butenyl)acetophenone

Emilio Lizárraga [a], Elida Romano [b], Roxana Amelia Rudyk [b], César Atilio Nazareno Catalán [a], Silvia Antonia Brandán [b,*]

[a] INQUINOA-CONICET, Instituto de Química Orgánica, Facultad de Bioquímica Química y Farmacia, Universidad Nacional de Tucumán, Ayacucho 471, 4000 San Miguel de Tucumán, Argentina
[b] Cátedra de Química General, Instituto de Química Inorgánica, Facultad de Bioquímica, Química y Farmacia Universidad Nacional de Tucumán, Ayacucho 471, 4000 San Miguel de Tucumán, Argentina

HIGHLIGHTS

- Vibrational spectra of 4-hydroxy-3-(3-methyl-2-butenyl)acetophenone were registered.
- Seven stable conformers have been theoretically determined.
- A complete assignment of the observed spectral features is proposed.
- The theoretical calculations allowed obtaining a set of scaled force constants.
- The nature of the phenyl ring was studied by NBO and AIM analysis.

GRAPHICAL ABSTRACT

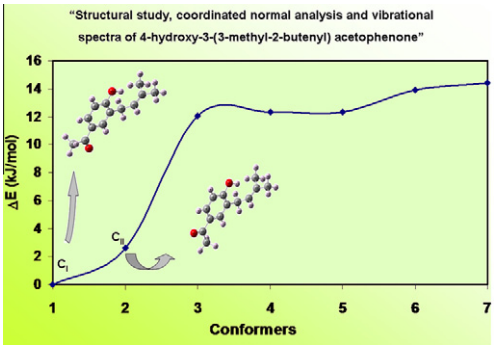

ARTICLE INFO

Article history:
Received 18 April 2012
Received in revised form 30 May 2012
Accepted 6 June 2012
Available online 13 June 2012

Keywords:
4-Hydroxy-3-(3-methyl-2-butenyl)acetophenone
Vibrational spectra
Molecular structure
Force field
DFT calculations

ABSTRACT

Structural and vibrational properties of 4-hydroxy-3-(3-methyl-2-butenyl)acetophenone, isolated from *Senecio nutans* Sch. Bip. (Asteraceae) were studied by infrared and Raman spectroscopies in solid phase. The Density Functional Theory (DFT) method together with Pople's basis set show seven stable conformers for the compound in the gas phase and that only two conformations are probably present in the solid phase. The harmonic vibrational wavenumbers for the optimized geometry were calculated at B3LYP/6-31G* and B3LYP/6-311++G** levels. For a complete assignment of the vibrational spectra, DFT calculations were combined with Pulaý's Scaled Quantum Mechanics Force Field (SQMFF) methodology in order to fit the theoretical wavenumber values to the experimental ones. Then, a complete assignment of all the observed bands in the vibrational spectra was performed. The natural bond orbital (NBO) study reveals the characteristics of the electronic delocalization of the two stable structures, while the corresponding topological properties of electronic charge density were analyzed by employing *Bader's* Atoms in the Molecules theory (AIM).

Introduction

Compounds containing furan [1–3], benzyl [4–9], imidazol [1–4], lactone [10,11] and oxadiazole [12] rings in their structures were recently studied from a structural and spectroscopic point of view because many of them possess interesting properties. In this work, we have studied the structural and vibrational properties of 4-hydroxy-3-(3-methyl-2-butenyl)acetophenone because, so far, its crystal and molecular structure has not been determined and there is no theoretical study concerning either its geometry or vibrational spectra. 4-Hydroxy-3-(3-methyl-2-butenyl)acetophenone was described for the first time by Bohlmann et al. [13] as a constituent of *Helianthella uniflora* and later isolated from *Senecio*

* Corresponding author. Tel.: +54 381 4247752; fax: +54 381 4248169.
E-mail address: sbrandan@fbqf.unt.edu.ar (S.A. Brandán).

1386-1425/$ - see front matter © 2012 Elsevier B.V. All rights reserved.
http://dx.doi.org/10.1016/j.saa.2012.06.004

graveolens (syn. *Senecio nutans*) [14,15], *Helichrysum italicum* [16], *Xenophyllum poposum* [17] and *Xenophyllum incisum* [18]. Structural and vibrational studies of this compound, isolated from *S. nutans* Sch. Bip. (Asteraceae), are of pharmacological interest because this prenylated acetophenone derivative proved to be an effective antifungal agent possessing also a moderate antibacterial activity [16]. Moreover, it is known that prenylated *p*-hydroxyacetophenone derivatives are biogenetic precursors of benzofurans and benzochromenes, two significant groups of bioactive metabolites in the plant kingdom [19]. Here, an experimental and theoretical study of 4-hydroxy-3-(3-methyl-2-butenyl)acetophenone was performed in order to evaluate the best theory level and basis set to reproduce the experimental vibrational spectra and carry out their complete assignment. This way, the optimized geometries of the more stable structures and the corresponding frequencies for the normal vibration modes were calculated. The normal mode calculations were accomplished by using a generalized valence force field (GVFF). Here, the molecular force fields for the two most stable conformers were calculated by using the B3LYP/6-31G* and B3LYP/6-311++G** combinations. Additionally, the nature of the rings and the electronic properties of all conformers were evaluated by means of NBO [20], Atoms in Molecules (AIM) [21,22] and HOMO–LUMO studies.

Experimental methods

Crystalline 4-hydroxy-3-(3-methyl-2-butenyl)acetophenone (**HMBA**) was obtained from aerial parts of *Senecio nutans*. Leaves and flowers were extracted with chloroform at room temperature for 3 days. After solvent evaporation, the chloroform extract was chromatographed on silica gel Merck 230–400 mesh using hexane–ethyl acetate mixtures of increasing polarity (97:3, 95:5, 93:7, 90:10, 87:13: 85:15 and 80:20). Fractions showing a single spot on TLC were reunited and the solvent evaporated to yield HMBA as a crystalline solid. Two crystallizations from heptane-ethyl acetate 10:1 yielded an analytical sample (purity >99.98% by capillary GC) of HMBA, mp 95–96 °C (reported: 96 °C [18]; 80–82 °C [17]). UV, EI-MS, ^{1}H- and ^{13}C NMR spectra: identical to the reported [13,16,17]. HMBA was the main component of the chlorofom extract of *S. nutans*.

4-Hydroxy-3-(3-methyl-2-butenyl)acetophenone: needles mp 95–96 °C (after two crystallizations from heptane-ethyl acetate 10:1). Purity: >99.98% by capillary gas chromatography using both flame ionization detector (FID) and selective mass detector.

UV (EtOH 96°)) λmax (log ε 281 nm (4.139) and 226 nm (4.170). EIMS: *m*/*z* (rel. int.) $[M]^+$ 204 (36), 189 (M-Me; 50), 161 (15), 149 (63), 147 (12), 145 (9), 133 (43), 128 (5), 127 (4), 115 (10), 106 (6), 105 (6), 91 (15), 77 (16), 51 (10), 43 (100). ^{1}H NMR (200 MHz, $CDCl_3$) δ: 8.1 2 br s, OH, 7.8 0 δ, 2.2 Hz, H-2), 7.75 (dd, 8.3 and 2.2 Hz, H-6), 6.93 (d, 8.3 Hz, H-5), 5.33 (br t, 7.2 Hz, H-2'), 3.39 (2H, br d, 7.2 Hz, H-1'), 2.58 (3H, s, H-2''), 1.74 (6H, br s). ^{13}C NMR ($CDCl_3$) δ: 198.8 (s, C-1''), 159.8 (s, C-4), 134.0 (s, C-3'), 130.8 (d, C-2), 129.3 (s, C-1), 128.8 (d, C-6), 128.0 (s, C-3), 121.3 (d, C-2'), 115.2 (d, C-5), 28.7 (t, C-1'), 26.1 (q, C-2''), 25.6 and 17.7 (both q, C-4' and C-5').

Nuclear magnetic resonance (NMR) spectra were recorded on a Bruker 300 AVANCE spectrometer at 300 MHz for 1H and 75 MHz for ^{13}C in $CDCl_3$ solutions containing TMS as internal standard. GC–MS spectrum was recorded on a 5973 Hewlett–Packard selective mass detector coupled to a Hewlett Packard 6890 gas chromatograph equipped with a Perkin-Elmer Elite-5MS capillary column (5% phenyl methyl siloxane, length = 30 m, inner diameter = 0.25 mm, film thickness = 0.25 μm); ionization energy, 70 eV; carrier gas: Helium d at 1.0 mL/min. UV spectra were run on a UV–Visible 160 A Shimadzu spectrophotometer.

The FT-IR spectrum in the region of 4000–400 cm^{-1} was recorded on a Bruker IFS 66/S spectrometer in KBr pellets at room temperature. Raman spectrum was measured on the substance contained in a glass capillary between 4000 and 100 cm^{-1} with a Bruker RF100/S spectrometer provided with a Nd:YAG laser (excitation line of 1064 nm, 800 mW of laser power) and a Ge detector cooled at liquid nitrogen temperature. The spectra were recorded with a resolution of 1 cm^{-1} and 200 scans.

Computational details

The potential energy curves for **HMBA** described by the C4–C3–C18–C21, C3–C18–C21–C22, C5–C4–O16–H17 and C6–C1–C10–C12 dihedral angles were studied at the B3LYP/6-31G* and 6-311++G** levels. In both calculations, seven stable conformations (C_I, C_{II}, C_{III}, C_{IV}, C_V, C_{VI} and C_{VII}) with C_1 symmetries were obtained according to the spatial orientation of the different three substituents groups on the aromatic ring. The structures of all conformers and atoms labeling can be seen in Figs. 1a and b. Natural charges and bond orders were also calculated at the same theory levels for all the structures from NBO calculation by using the NBO 3.1 program [23], as implemented in the GAUSSIAN 03 package [24]. The electronic charge density topological analysis was performed for those stable structures, by using the AIM200 program package [22]. The harmonic wavenumbers and the resulting force fields

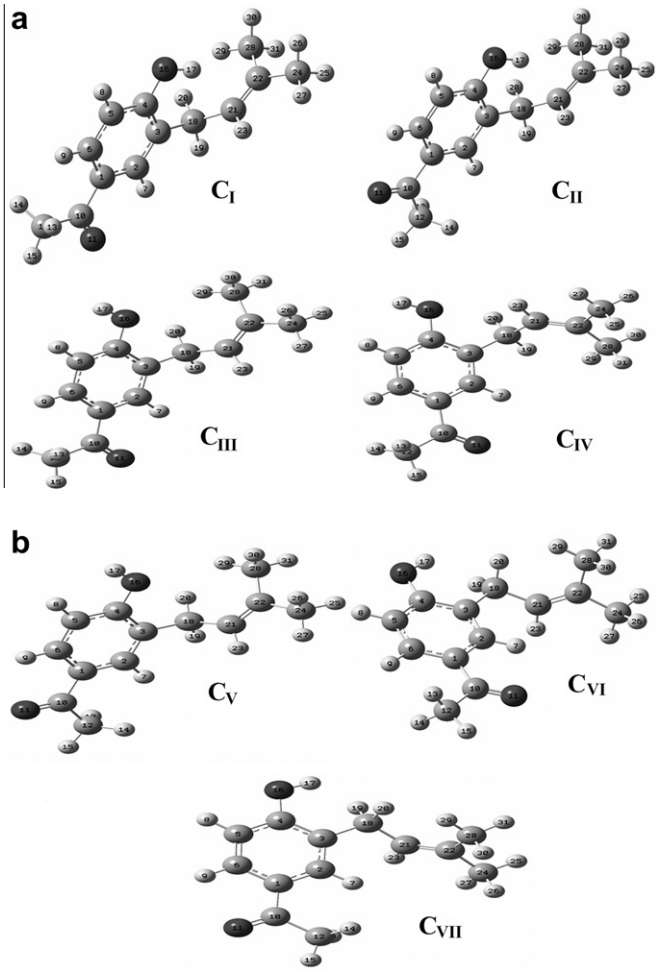

Fig. 1. Molecular structures of 4-hydroxy-3-(3-methyl-2-butenyl)acetophenone and atoms numbering: a) From C_I to C_{IV} conformers and, b) From C_V to C_{VII} conformers.

were transformed to "natural" internal coordinates by using the MOLVIB program [25]. The natural internal coordinates for **HMBA** have been defined according to those reported in the literature [6,7], and are listed in Table S1 (Supporting Material). Following the SQMFF procedure [26], the harmonic force fields for those structures were evaluated at the B3LYP/6-31G* level. The potential energy distribution components (PED) higher than or equal to 10% are subsequently calculated with the resulting SQM. The nature of all the vibration modes was determinate by means of the *Gauss-View* program [27].

Results and discussion

Geometry optimization

A comparison of the total energies and the corresponding dipole moment values for all the stable structures by using both methods are given in Table S2. The results show that the energies of the C_I and C_{II} conformers are significantly lower than the corresponding to the other five conformers (C_{III} thru C_{VII}), and that the difference of potential energy between conformers C_I and C_{II} by using B3LYP/6-31G* and B3LYP/6-311++G** methods are respectively 2.62 and 2.88 kJ/mol. On the other hand, the high value of the dipolar moment for the C_{II} conformer could partly explain its stability, as was observed in other molecules [7,28,29]. Table 1 shows a comparison of the calculated geometrical parameters for all the structures of **HMBA**, by using the B3LYP/6–31G* calculations, with the two structures of 4-hydroxyacetophenone (forms I and II) determined by X-ray diffraction by Bernardes et al. [30]. In general, the theoretical values for all the conformers are in agreement with the experimental values for the form I of 4-hydroxyacetophenone. The dihedral angles for all the conformers are given in Table S3 and they show that the C6–C1–C10–C12 dihedral angle is different in the two most stable conformers. Hence, the energy calculation predicts that the C_I and C_{II} conformers are the most stable and that probably both conformers are present in the crystalline state.

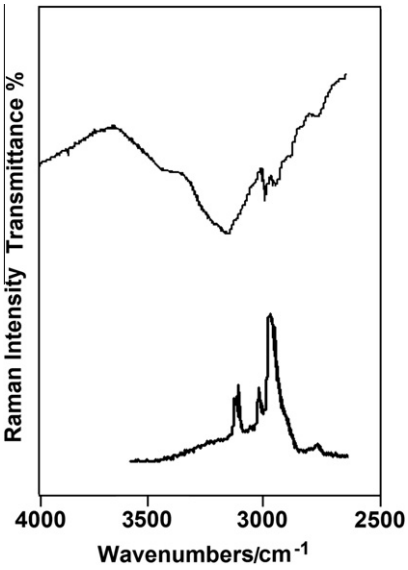

Fig. 2. Experimental infrared (upper; KBr pellet) and Raman (bottom) spectra of crystalline 4-hydroxy-3-(3-methyl-2-butenyl)acetophenone in the 4000–2500 cm^{-1} region.

NBO, electrostatic potential and AIM Studies

The stabilities of the C_I and C_{II} conformers of **HMBA** in relation to the other ones were investigated by using NBO calculations [20],

Table 1
Comparison of calculated geometrical parameters for the conformers of 4-hydroxy-3-(3-methyl-2-butenyl)acetophenone.

Parameter	B3LYP/6-31G*[a]							Exp.[b]	
	I	II	III	IV	V	VI	VII	Form I	Form II
Bond lengths (Å)									
O16–C4	1.360	1.360	1.365	1.367	1.365	1.365	1.365	1.370(2)	1.359(3)
C3–C4	1.414	1.412	1.411	1.410	1.408	1.412	1.410	1.382(2)	1.379(4)
C3–C2	1.391	1.396	1.390	1.390	1.394	1.391	1.395	1.383(2)	1.371(4)
C2–C1	1.404	1.403	1.406	1.406	1.405	1.405	1.403	1.395(2)	1.378(3)
C6–C1	1.404	1.406	1.401	1.401	1.403	1.403	1.405	1.402(2)	1.387(3)
C6–C5	1.389	1.385	1.392	1.392	1.387	1.389	1.385	1.378(2)	1.370(4)
C4–C5	1.400	1.402	1.399	1.399	1.401	1.398	1.401	1.389(2)	1.372(4)
C10–C1	1.491	1.491	1.492	1.492	1.492	1.492	1.492	1.486(2)	1.465(3)
C10–C12	1.522	1.523	1.523	1.522	1.522	1.523	1.523	1.492(3)	1.494(4)
C10–O11	1.224	1.224	1.224	1.223	1.224	1.224	1.224	1.231(2)	1.226(3)
RMSD	0.0050	0.0050	0.0048	0.0047	0.0046	0.0048	0.0047		
RMSD	0.0072	0.0073	0.0072	0.0071	0.0071	0.0071	0.0071		
Bond angles (°)									
O16–C4–C3	122.4	122.4	117.2	117.0	117.2	122.4	122.5	122.9(1)	117.5(3)
O16–C4–C5	117.0	117.0	121.8	121.9	121.8	116.6	116.5	117.1(2)	122.7(2)
C2–C3–C4	117.9	117.9	117.6	117.5	117.6	117.7	117.8	119.7(1)	119.8(3)
C3–C2–C1	122.4	122.3	122.6	122.6	122.4	122.3	122.1	121.6(2)	121.2(3)
C6–C1–C2	118.3	118.3	118.4	118.5	118.4	118. 6	118.6	117.6(1)	118.1(2)
C5–C6–C1	120.6	120.7	120.3	120.3	120.4	120.5	120.6	121.1(1)	121.0(2)
C5–C4–C3	120.6	120.6	120.9	121.1	121.0	121.0	121.0	120.0(1)	119.7(2)
C4–C5–C6	120.2	120.1	120.1	120.1	120.1	119.9	119.9	120.0(2)	120.1(2)
C6–C1–C10	123.3	118.6	118.4	123.1	118.4	123.2	118.5	119.3(1)	119.4(2)
C2–C1–C10	118.3	123.1	118.4	118.4	123.2	118.3	122.9	123.1(2)	122.4(2)
C1–C10–C12	118.8	119.0	118.8	118.8	118.9	118.8	118.9	120.0(2)	120.1(3)
O11–C10–C1	121.1	121.0	121.0	121.0	120.9	121.1	120.9	120.0(2)	120.5(2)
C12–C10–O11	120.1	120.1	120.2	120.2	120.2	120.1	120.1	120.0(2)	119.4(2)
RMSD	0.67	0.23	0.92	1.01	0.79	0.68	0.27		
RMSD	0.97	0.80	0.52	0.64	0.33	1.00	0.85		

[a] This work.
[b] For 4-Hydroxyacetophenone taken from [27].

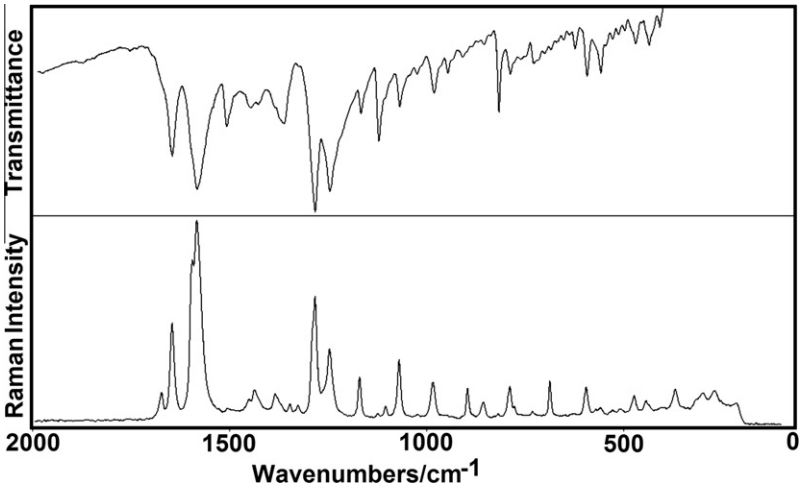

Fig. 3. Experimental infrared (upper; KBr pellet) and Raman (bottom) spectra of crystalline 4-hydroxy-3-(3-methyl-2-butenyl)acetophenone in the 1800–0 cm^{-1} region.

molecular electrostatic potential and Bader's charge electron density topological analysis [21]. The atomic charges (NPA) for all conformers of **HMBA** by using both basis sets are given in Tables S4 and S5, respectively. The results with those basis sets show that the stabilities of C_I and C_{II} are associated to the high atomic charges values of the O11, O16, C18 and C22 atoms, in reference to the other ones. The calculated molecular electrostatic potentials by using 6-31G* and 6-311++G** basis sets are summarized in Tables S6 and S7, respectively. For the C_I structure, the lower molecular electrostatic potential values are observed for the C6, C22, C24, C28, H29, H30 and H31 atoms, while for the O16 atoms the values are higher. Moreover, the O11 atoms have higher electrostatic potential values than the O16 atoms, as could be expected, because the former are involved in a double bond and, for this, their $\Delta ET_{LP\rightarrow\sigma^*}$ charge transfers have lower values than those corresponding to the O16 atoms, as it will be seen later. In the NBO analysis, for all **HMBA** conformers, the second order perturbation energies $E^{(2)}$ (donor → acceptor) involving the most important delocalization are presented in Table S8. The results with both calculation levels show that the interactions between the lone-pair orbitals ($\Delta ET_{LP\rightarrow\sigma^*}$ charge transfers) and their C–C filled orbitals are the most energetic steric repulsions. Here, the hyperconjugation between the electron donating groups and the phenyl ring shows these larger energies. These result revels that the $\Delta ET_{\sigma\rightarrow\sigma^*}$ and $\Delta ET_{LP\rightarrow\sigma^*}$ charge transfers stabilize respectively to the C_I and C_{II} conformers but, this analysis does not explain the large differences in energies with the remaining conformers. On the other hand, the topological properties, such as the calculated charge electron density, (ρ) and the *Laplacian* values, $\nabla^2\rho(r)$ in the bond critical points (BCPs) and the ring critical points (RCPs) for all the structures are shown in Table S9. This analysis, by using both basis sets, shows important differences among the topological properties of all conformers. A difference is that the C_I, C_{II}, C_{VI} and C_{VII} conformers show two BCPs and three RCPs where the topological properties for the C_I and C_{II} conformers are completely different, in nature and values, to those corresponding to the C_{VI} and C_{VII} conformers. Therefore, for the two first conformers, the two BCPs are observed between the C21···H17 and H20···H29 atoms, while for the other ones, those BCPs are observed between the C18···H17 and H20···H29 atoms. Note that the densities values in the C21···H17 BCPs of C_I and C_{II} have higher values than the other C18···H17 BCPs corresponding to C_{VI} and C_{VII} while the distances between those involved atoms are lower in the first two conformers, being lower in C_I (2.156 Å). These observations justify the stabilities of the C_I and C_{II} conformers in relation to the C_{VI} and C_{VII} conformers. Another difference observed between the C_{III} and C_V conformers are the two BCPs and three RCPs by using 6-31G* basis set while, by using the other basis set, only one BCP and two RCPs are observed. In these conformers, the two BCPs, by using 6-31G* basis set, are observed between the O16···H29 and H20···H29 atoms while only the H20···H29 BCP is observed in both conformers by using the other basis set. This way, the observed higher distances between the atoms involved in the BCPs (2.385–2.883 Å) explain the higher difference energies values among the C_{III}, C_{IV}, C_V, C_{VI} and C_{VII} conformers and, since their lower stabilities.

Vibrational analysis

Based on the above results, the C_I and C_{II} conformers of **HMBA** were considered. The recorded infrared and Raman spectra for the compound in solid phase can be seen in Figs. 2 and 3 respectively. Both conformers have 87 normal vibration modes, all active in the infrared and Raman spectra. The vibrational assignment of the experimental bands to the normal vibration modes is based on the comparison with related molecules [1–12] and with the results of the calculations performed here. Table 2 shows the experimental and calculated frequencies, the SQM based on the 6-31G* basis set, and the assignment for **HMBA**. We considered B3LYP/6-31G* calculations because the used scale factors are defined for this basis set (See Tables S10 and S11). The theoretical calculations reproduce the normal frequencies for the C_I and C_{II} conformers of **HMBA** with initial values of RMSDs of 14.1 and 14.2 cm^{-1}, respectively. When the SQMFF method is applied using the Pulay's scaling factors, the final RMSDs, decrease significantly until 7.9 cm^{-1} for both conformers by using the 6-31G* basis set. The SQM force fields for both structures of **HMBA** can be obtained at request. Below, we discuss the assignment of the most important groups.

Bands assignments

OH modes

The broad band observed in the IR spectrum of the compound in the solid phase at 3437 cm^{-1} is easily assigned to the O–H stretching mode for both conformers of **HMBA** according to the values reported for similar compounds [4,7,9]. Taking into account the assignations of similar molecules [4,7] and the theoretical calculations, the OH in-plane deformation modes for both conformers are assigned to the strong IR band at 1245 cm^{-1} while the corresponding out-of-plane deformation modes are associated with the very weak IR band at 497 cm^{-1}.

Table 2
Observed and calculated frequencies (cm^{-1}) using B3LYP method, and assignment 4-hydroxy-3-(3-methyl-2-butenyl)acetophenone.

Experimental		C_I				C_{II}			
IR[a]	Raman[a]	SQM[b]	IR[c] int.	Raman[d]	Assignment	SQM[b]	IR[c] int.	Raman[d]	Assignment
3437 w		3456	448.1	359.9	ν (O16–H17)	3462	428.5	348.4	ν (O16–H17)
3143 s		3086	10.5	155.7	ν_s C–H	3095	4.3	120.2	ν_s C–H
	3069 m	3073	4.4	42.1	ν (C2–H7)	3078	3.8	88.4	ν_{as} C–H
		3071	5.9	50.7	ν_{as} C–H	3058	10.3	42.4	ν (C2–H7)
	3058 m	3037	14.8	115.9	ν_{as} CH_3 (C12)	3037	15.3	122.1	ν_{as} CH_3
	3032 vw	3018	29.9	32.4	ν $_{as}$ CH_3 (C28)	3017	30.6	31.3	ν_{as} CH_3
	3012 vw	3014	15.9	70.0	ν (C21–H23)	3014	15.2	70.3	ν (C21–H23)
	3006 w	3000	15.4	42.9	ν_{as} CH_3 (C24)	3000	15.2	42.9	ν_{as} CH_3
	2990 sh	2983	11.2	50.6	ν_{as} CH_3(C12)	2982	11.8	41.8	ν_{as} CH_3
2971 s	2973 m	2955	29.1	183.7	ν_{as} CH_3(C28)	2956	28.8	183.0	ν_{as} CH_3
	2960 vw	2951	5.4	37.9	ν_{as} CH_3(C24)	2951	5.3	36.7	ν_{as} CH_3
	2960 vw	2945	14.4	72.1	ν_{as} CH_2	2942	16.5	79.3	ν_{as} CH_2
2929 s	2926 m	2926	3.3	118.6	ν_s CH_3(C12)	2925	3.7	106.8	ν_s CH_3
	2926 m	2915	45.0	408.7	ν_s CH_3 (C28)	2914	45.0	374.9	ν_s CH_3
	2926 m	2911	19.0	11.2	ν_s CH_2	2907	28.8	18.3	ν_s CH_2
2855 s	2893 sh	2906	20.6	92.2	ν_s CH_3 (C24)	2906	11.0	113.1	ν_s CH_3
1666 sh	1672 m	1703	170.7	81.1	ν (C10–O11)	1703	209.7	100.5	ν (C10–O11)
1646 s	1646 s	1667	8.6	64.2	ν (C21–C22)	1667	7.6	66.5	ν (C21–C22)
	1596 s	1606	157.4	146.3	ν_s C–C	1613	93.3	94.7	ν_s C–C
1583 s	1583 vs	1582	40.5	40.5	ν_s C–C	1574	121.0	88.0	ν_s C–C
1507 m	1506 w	1496	70.4	1.7	β C5–H8	1499	45.7	2.1	β C5–H8
		1461	4.4	76.4	δa CH_3 (C24)	1461	4.9	77.0	δa CH_3 (C24)
		1455	13.6	1.2	δa CH_3 (C28)	1456	14.5	1.3	δa CH_3 (C28)
	1452 w	1451	8.2	4.0	δa CH_3 (C28)	1451	7.5	4.1	δa CH_3 (C28)
1446 m		1443	8.8	25.1	δa CH_3 (C12)	1443	9.0	23.6	δa CH_3 (C12)
	1437 m	1437	0.3	31.9	δa CH_3 (C24)	1437	0.1	32.4	δa CH_3 (C24)
	1437 m	1435	8.7	11.4	δa CH_3 (C12)	1436	10.3	10.5	δa CH_3 (C12)
	1437 m	1431	5.6	2.1	δ CH_2	1430	3.5	1.6	δ CH_2
1427 m	1428 sh	1427	24.7	5.9	ν_{as} C–C	1422	26.3	11.8	ν_{as} C–C
1386 sh	1384 m	1389	1.8	38.0	δs CH_3 (C28)	1389	0.6	35.5	δs CH_3 (C28)
	1373 sh	1379	8.1	22.0	δs CH_3 (C24)	1379	9.0	21.5	δs CH_3 (C24)
1362 m		1365	22.1	3.3	ρ C21–H23	1364	2.0	4.9	ρ C21–H23
1362 m		1350	46.8	7.8	ν_{as} C–C	1349	63.5	6.7	δs CH_3 (C12)
	1348 w	1347	3.9	23.7	δs CH_3 (C12)	1345	5.5	26.6	ν_{as} C–C
	1326 w	1310	43.7	17.9	ρ CH_2	1312	13.4	2.3	β C2–H7
1283 vs	1285 s	1289	96.5	31.6	ν_{as} C–C	1290	107.1	42.3	ρ CH_2
1283 vs		1274	165.4	19.4	ν (C4–O16)	1280	112.6	13.6	ν (C4–O16)
	1256 sh	1267	33.2	23.0	ν (C1–C10)	1268	71.6	34.1	ν (C1–C10)
1245 s	1246 m	1220	81.1	18.2	wag CH_2	1223	233.1	10.0	wag CH_2
1245 s		1201	132.2	2.0	δ (O–H)	1207	5.1	9.3	δ (O–H)
1167 m	1170 m	1170	13.9	4.9	ν_{as} C–C	1170	5.3	6.7	ν_{as} C–C
	1170 m	1158	6.3	7.4	ν (C3–C18)	1153	4.8	4.4	ν (C3–C18)
1121 s	1123 vw	1115	6.5	5.6	β C6–H9	1106	6.1	7.7	β C6–H9
		1100	26.1	12.4	ν (C18–C21)	1099	26.2	9.6	ρ′ CH_3(C24)
1103 sh	1104 w	1090	1.9	0.4	ρ CH_3(C28)	1090	1.6	0.3	ρ′ CH_3(C28)
1068 s	1070 m	1067	4.4	16.3	β C2–H7	1069	7.4	26.1	ν_{as} C–C
1044 sh	1031 vw	1033	1.5	1.8	ρ CH_3 (C12)	1034	1.6	1.9	ρ CH_3 (C12)
1023 w	1021 vw	1014	1.3	8.5	ρ CH_3(C24)	1013	0.9	8.6	ν (C18–C21)
	1010 vw	1007	4.6	1.4	ρ CH_3 (C24)	1006	4.4	1.4	ρ CH_3 (C24)
981 w	983 m	963	19.6	7.8	ρ CH_3(C12)	979	0.6	0.6	γ C6–H9
962 sh		948	0.6	3.0	γ C6–H9				
946 w	948 sh	945	17.3	2.4	ρ CH_3 (C28)	945	0.3	2.9	ρ CH_3 (C28)
933 sh	938 vw	941	7.5	2.1	γ C2–H7	939	36.4	7.4	ρ′ CH_3(C12)
908 w	908 sh					913	29.6	3.8	β R_1
	895 m	906	30.7	3.5	γ C21–H23	907	8.3	4.7	γ C21–H23
885 vw	882 vw	883	2.7	8.4	ν (C10–C12)	891	7.4	2.1	γ C2–H7
854 vw	855 w	848	10.1	14.4	τw CH_2	850	7.9	11.8	γ C5–H8
816 m	818 vw					845	21.6	3.7	τw CH_2
787 w	789 m	831	22.3	2.3	γ C5–H8				
776 sh	778 sh	771	7.9	3.7	ν_s C–C	776	6.1	3.7	ν_s C–C
744 sh	745 vw	741	3.3	16.6	ν_s C–C	742	1.9	18.1	ν_s C–C
727 w	731 vw	727	1.2	0.4	τR_1	728	1.6	0.6	τR_1
684 vw	687 m	681	1.7	4.6	β R_1	679	0.7	6.1	ν (C10–C12)
623 vw	625 vw	641	3.0	3.0	β R_3	640	2.3	2.5	β R_3
592 w	595 m	610	3.4	4.6	γ C10–O11	610	5.4	2.4	γ C10–O11
	570 w					587	23.5	2.1	ρ C10–O11
557 w	558 w	569	42.7	0.9	ρ C10–O11				
543 sh	534 vw	534	72.9	5.4	ρ C22–C28	526	68.8	4.4	ρ C22–C28
527 w	527 w	518	3.2	1.0	τR_3, τR_1, γC4–O16				
512 vw	510 w	501	0.5	0.6	γ C4–O16	511	4.6	0.8	γ C4–O16
497 vw	490 sh	490	5.6	1.5	τ OH	498	7.2	2.6	τ OH
477 sh	472 m					479	15.7	0.4	β C4–O16
469 vw		460	3.2	2.4	γ C21–C22				

Table 2 (*continued*)

Experimental		C_I				C_{II}			
IR[a]	Raman[a]	SQM[b]	IR[c] int.	Raman[d]	Assignment	SQM[b]	IR[c] int.	Raman[d]	Assignment
452 vw	457 sh					455	1.1	1.4	γ C21–C22
441 vw	442 w	441	0.7	2.9	γ C3–C18				
435 vw	435 sh					440	0.7	2.4	γ C3–C18
407 vw	401 w	402	0.7	0.3	δ C24–C22–C28	407	2.7	1.5	δ C12–C10–C1
	394 w	401	0.3	0.5	β C4–O16	403	0.4	0.3	δ C24–C22–C28
	369 m	343	0.7	1.7	β R_2				
	336 w					336	1.7	2.5	β R_2
	317 w	309	0.2	3.8	τ R_2	314	1.2	2.4	τ R_2
	297 m	286	1.5	0.7	β C3–C18	288	1.4	0.8	β C3–C18
	269 m	274	2.6	1.1	τ C22–C24	274	4.0	1.2	τ C22–C24
	251 sh					243	3.7	3.6	δ C12–C10–C1
	235 w	238	1.7	3.7	δ C18–C21–C22; δ C12–C10–C1				
	212 w	196	0.3	1.2	τR_3	193	0.5	1.5	τR_3
	163 vvw	171	1.4	0.9	τw CH_3 (C24)	170	1.8	1.2	τw CH_3 (C24)
		150	0.3	0.0	β C1–C10	149	0.2	0.2	β C1–C10
	136 vvw	140	4.7	1.9	τw CH_3 (C12)	141	1.1	1.6	τw CH_3 (C12)
		122	0.6	0.4	τw CH3 (C28)	122	0.5	0.4	τw CH3 (C28)
		110	1.4	0.6	γ C1–C10	112	1.6	0.4	γC1–C10
		81	0.5	2.9	δ CCC	82	0.4	3.2	δ CCC
		53	4.0	0.9	τw O11–C1–C12	51	2.1	0.9	τw O11C10C12
		38	0.3	2.2	τ C18–C3	38	0.8	2.0	τ C18–C3
		32	0.4	0.9	τ C18–C21	32	0.3	1.1	τ C18–C21

ν, stretching; δ, scissoring; wag, wagging; γ, out-of plane deformation; ρ, in-plane deformation or rocking; τ, torsion, τw, twisting; a, antisymmetric; s, symmetric.
[a] This work.
[b] From scaled quantum mechanics force field at B3LYP/6-31G* level.
[c] Units are km.mol^{-1}.
[d] Raman activities in Å^4 (amu)$^{-1}$.

Table 3
Scaled force constants for both conformers of 4-hydroxy-3-(3-methyl-2-butenyl)acetophenone at different theory levels.

B3LYP				
Description	6-31G*		6-311++G**	
	I	II	I	II
f (νO–H)	6.68	6.70	6.92	6.95
f (νC=O)	11.61	11.63	11.23	11.26
f (νC–O)	6.19	6.18	5.84	5.83
f (νC–C)$_R$	6.46	6.45	6.32	6.32
f (νC=C)	6.11	8.63	6.00	8.44
f (νC–H)$_R$	5.20	5.20	5.12	5.12
f (νCH_3)	4.86	4.85	4.78	4.78
f (νCH_2)	4.74	4.73	4.69	4.68
f (νC–CH_3)	4.10	4.10	4.04	4.04
f (δCH_2)	0.77	0.77	0.74	0.74
f (δCH_3)	0.63	0.55	0.52	0.52
f (δOH)	0.84	0.84	0.79	0.78

Units in mdyn Å^{-1} for stretching and mdyn Å rad^{-2} for angle deformations Abbreviations, ν, stretching; , deformation in the plane.

CH_3 modes

Here, the antisymmetric and symmetric stretching modes of methyl groups are calculated as totally pure modes, hence, they are easily assigned between 3058 and 2855 cm^{-1}. The antisymmetric and symmetric CH_3 bending modes are predicted by calculations between 1461 and 1347 cm^{-1}; for this reason, they were assigned in this region. The rocking and twisting modes are clearly predicted in the expected regions [7] for both structures of **HMBA**, thus, they were assigned in those regions, as observed in Table 2.

CH modes

The C–H stretching modes are assigned between 3143 and 3012 cm^{-1}, as observed in Table 2. The two in-plane deformation modes for both conformers were assigned to the IR bands at 1507 and 1121 cm^{-1} while the remaining modes are assigned to the Raman band at 1326 cm^{-1}, for the C_{II} conformer and to the IR band at 1068 cm^{-1}, for the C_I conformer. The IR bands at 981, 885, 854 and 787 cm^{-1} and the shoulders located at 962 and 933 cm^{-1}, were assigned to the corresponding out-plane deformation modes.

CH_2 modes

The two stretching modes of this group can be assigned to the Raman bands respectively at 2960 and 2926 cm^{-1} for both conformers while the CH_2 bending modes for the two conformers are associated with the Raman band of medium intensity at 1437 cm^{-1}. Both wagging modes were predicted at 1220 and 1223 cm^{-1}, for this reason, they are easily assigned to the strong IR band at 1245 cm^{-1}. The Raman bands at 1326 and 1246 cm^{-1} are assigned to the expected rocking modes, as indicated in Table 2, while the twisting modes are associated with the IR bands at 854 and 816 cm^{-1}.

Skeletal modes

In both conformers of **HMBA**, the C=C stretching corresponding to the prenyl side chain are assigned to the strong IR band at 1646 cm^{-1}. In accordance with the values previously reported for molecules with a similar ring [1–9] and our theoretical results, the bands at 1596, 1583, 1427,1362, 1348, 1167 and 1068 cm^{-1} and the shoulders at 776 and 744 cm^{-1} are assigned to the skeletal stretching modes of the molecule, as can be seen in Table 2. According to a previous assignment for *p*-hydroxy acetophenone [31], the carbonyl stretching mode splits into two components in the infrared at 1652 and 1645 cm^{-1}. The splitting is probably due to intermolecular association based on C=O···H–O type hydrogen bonding [31]. Thus, the shoulder and the strong band respectively at 1666 and 1646 cm^{-1} can be assigned to the C=O stretching modes of both conformers while the very strong band at 1283 cm^{-1} is associated with the C–O stretching modes. A similar IR spectrum of HMBA in CCl_4 solution was registered (see Figure S1). Here, the different intensities calculated for the C=O stretching modes of both conformers are attributed to the molecular

orbital bond order, which values are respectively 0.3980 (C1–O10) and 0.7326 (C21–C22) for C_I and 1.4553 (C1–O10) and 0.7974 (C21–C22) for C_{II}. The phenyl ring deformations for both conformers of **HMBA** are associated with the IR bands observed at 908, 684 and 623 cm^{-1} and with the Raman bands at 369 and 336 cm^{-1} while the IR band at 727 cm^{-1} and the Raman bands at 317 and 212 cm^{-1} were assigned to the ring torsion modes For the C_I conformer the calculations predicted two ring torsion modes coupled with the C4–O16 out-of-plane deformation at 527 cm^{-1}. The remaining skeletal modes were assigned as can be seen in Table 2.

Force field

For **HMBA**, the force constants expressed in terms of simple valence internal coordinates were calculated from the corresponding scaled force fields by using the MOLVIB program [25] and the SQM methodology [26] as was described in computational details. The calculated values for both conformers at the B3LYP/6-31G* level are shown in **Table 3**. In general, the force constant values, by using the two basis sets, are similar for both conformers of **HMBA** with exception of the *f(υC=C)* force constants that in the C_{II} conformer has a higher value than the C_I conformer. These differences in the values are justified by the bond order between the involved atoms because in the C_I conformer the C21 and C22 atoms have bond orders of 3.0325 and 3.1809 respectively while in the C_{II} conformer the bond orders are respectively 3.9507 and 4.0022. Thus, the C21···H17 bond in the first conformer is stronger than in the second one and hence, the C21=C22 bond is weak in C_I and strong in C_{II}, in accordance with the corresponding force constants. The weakness of the C21=C22 double bond in the C_I conformer is in agreement with an easy attack of a phenolic hydroxyl at C21 and C22 to generate benzofurans and benzopyranes derivatives respectively.

HOMO–LUMO study

The calculated frontier molecular HOMO and LUMO orbitals for all conformers of **HMBA** are given in Table S12. The results show that both orbitals are mainly localized on the phenyl ring, indicating that the HOMO–LUMOs are mostly π-antibonding type orbitals. The large HOMO–LUMOs gaps for the C_{VI} and C_{VII} conformers means high excitation energies for many excited states, good stabilities and have a high chemical hardness while the C_{IV} conformer is more polarizable with a high chemical reactivity.

Conclusions

The characterization of 4-hydroxy-3-(3-methyl-2-butenyl) acetophenone was performed by means of infrared and Raman spectroscopic techniques. The molecular structures of 4-hydroxy-3-(3-methyl-2-butenyl)acetophenone by the B3LYP/6-31G* and B3LYP/6-311++G** methods suggest the existence of seven stable structures in the gas phase. The presence of the C_I and C_{II} conformers was detected in both spectra, and a complete assignment of the vibrational modes was accomplished. The B3LYP/6-31G* and B3LYP/6-311++G** SQM force fields were obtained for the two conformers of 4-hydroxy-3-(3-methyl-2-butenyl)acetophenone. The stabilities of both forms were justified by means of electrostatic potentials, NBO and AIM analyses. The HOMO–LUMO study shows that the C_I conformer has a greater energy gap than the C_{II} conformer, hence, C_I is more stable than C_{II} but, the stabilities of the remaining conformers are not justified by this analysis due to the remarkable differences between their values.

Acknowledgements

This work was supported with grants from CIUNT (Consejo de Investigaciones, Universidad Nacional de Tucumán), CONICET (Consejo Nacional de Investigaciones Científicas y Técnicas, R. Argentina) and ANPCYT PICT 0394. The authors thank Prof. Tom Sundius for his permission to use MOLVIB.

Appendix A. Supplementary data

Supplementary data associated with this article can be found, in the online version, at http://dx.doi.org/10.1016/j.saa.2012.06.004.

References

[1] A.E. Ledesma, J. Zinczuk, J.J. López González, A. Ben Altabef, S.A. Brandán, J. Mol. Struct. 322 (2009) 924–926.
[2] A.E. Ledesma, J. Zinczuk, A. Ben Altabef, J.J. López-González, S.A. Brandán, J. Raman Spectrosc. 40 (8) (2009) 1004–1010.
[3] C.D. Contreras, M. Montejo, J.J. López González, J. Zinczuk, S. Brandán, J. Raman Spectrosc. 42 (1) (2011) 108–116.
[4] C.D. Contreras, A.E. Ledesma, H.E. Lanús, J. Zinczuk, S.A. Brandán, Vib. Spectros. 57 (2011) 108–115.
[5] P. Leyton, J. Brunet, V. Silva, C. Paipa, M.V. Castillo, S.A. Brandán, Spectrochim. Acta, Part A 88 (2012) 162–170.
[6] C.D. Contreras, A.E. Ledesma, J. Zinczuk, S.A. Brandán, Spectrochim. Acta, Part A 79 (2011) 1710–1714.
[7] E. Romano, A.B. Raschi, A. Benavente, S.A. Brandán, Spectrochim. Acta, Part A 84 (2011) 111–116.
[8] A.E. Ledesma, C. Contreras, J. Svoboda, A. Vektariane, S.A. Brandán, J. Mol. Struct. 967 (2010) 159–165.
[9] S.A. Brandán, F. Marquez Lopez, M. Montejo, J.J. Lopez Gonzalez, A. Ben Altabef, Spectrochim. Acta, Part A 75 (2010) 1422–1434.
[10] L.C. Bichara, H.E. Lanús, C.G. Nieto, S.A. Brandán, J. Phys. Chem. A 114 (2010) 4997–5004.
[11] L.C. Bichara, H.E. Lanús, S.A. Brandán, J. Chem. Chem. Eng. 5 (2011) 936–945.
[12] E. Romano, N.A.J. Soria, R. Rudyk, S.A. Brandán, J. Mol. Simul. (2012) 1–6.
[13] F. Bohlmann, M. Grenz, Chem. Ber. 103 (1970) 90–96.
[14] L.A. Loyola, S. Pedreros, G. Morales, Phytochemical 24 (7) (1985) 1600–1602.
[15] S. Dupré, M. Grenz, J. Jakupovic, F. Bohlmann, H.M. Niemeyer, Phytochemecial 30 (4) (1991) 1211–1220.
[16] F. Tomás-Barberán, E. Iniesta-San Martín, F. Tomás-Lorente, A. Rumbero, Phytochemistry 29 (1990) 1093–1095.
[17] M.A. Ponce, E. Gross, An. Asoc. Quim. Argent 79 (5) (1991) 197–200.
[18] M.J.A. Marchese, S.S.de. Heluani, C.A.N. Catalán, C.A. Griffin, J.B. Vaughn, W. Herz, Biochem. Syst. Ecol. 35 (2007) 169–175.
[19] P. Proksch, E. Rodriguez, Phytochemistry 22 (1983) 2335–2348.
[20] A.E. Reed, L.A. Curtis, F. Weinhold, Chem. Rev. 88 (6) (1988) 899–926.
[21] R.F.W. Bader, Atoms in Molecules, Oxford University Press, Oxford, A Quantum Theory, 1990, ISBN 0198558651.
[22] F. Biegler-Köning, J. Schönbohm, D. Bayles, AIM2000; a program to analyze and visualize atoms in molecules, J. Comput. Chem. 22 (2001) 545.
[23] E.D. Glendening, J.K. Badenhoop, A.D. Reed, J.E. Carpenter, F. Weinhold, NBO 3.1; Theoretical Chemistry Institute, University of Wisconsin; Madison, WI, 1996.
[24] M.J. Frisch, G.W. Trucks, H.B. Schlegel, G.E. Scuseria, M.A. Robb, J.R. Cheeseman, J.A. Jr. Montgomery, T.Vreven, K.N. Kudin, J.C. Burant, J.M. Millam, S.S. Iyengar, J.Tomasi, V. Barone, B. Mennucci, M. Cossi, G. Scalmani, N. Rega, G.A. Petersson, H. Nakatsuji, M. Hada, M. Ehara, K. Toyota, R. Fukuda, J. Hasegawa, M. Ishida, T. Nakajima, Y. Honda, O. Kitao, H. Nakai, M. Klene, X. Li, J.E. Knox, H.P. Hratchian, J.B. Cross, C. Adamo, J. Jaramillo, R. Gomperts, R.E. Stratmann, O. Yazyev, A.J. Austin, R. Cammi, C. Pomelli, J.W. Ochterski, P.Y. Ayala, K. Morokuma, G.A. Voth, P. Salvador, J.J. Dannenberg, V.G. Zakrzewski, S. Dapprich, A.D. Daniels, M.C. Strain, O. Farkas, D.K. Malick, A.D. Rabuck, K. Raghavachari, J.B. Foresman, J.V. Ortiz, Q. Cui, A.G. Baboul, S. Clifford, J. Cioslowski, B.B. Stefanov, G. Liu, A. Liashenko, P. Piskorz, I. Komaromi, R.L. Martin, D.J. Fox, T. Keith, M.A. Al-Laham, C.Y. Peng, A. Nanayakkara, M. Challacombe, P.M.W. Gill, B. Johnson, W. Chen, M.W. Wong, C. Gonzalez, J.A. Pople, Gaussian 03, Revision B.01, Gaussian, Inc., Pittsburgh PA, 2003.
[25] T. Sundius, J. Mol. Struct. 218 (1990) 321–326.
[26] P. Pulay, G. Fogarasi, F. Pang, E. Boggs, J. Am. Chem. Soc. 101 (10) (1979) 2550.
[27] A.B. Nielsen, A.J. Holder, Gauss View 3.0, User's Reference, GAUSSIAN Inc., Pittsburgh, PA, 2000–2003.
[28] J.R. Sambrano, A.R. de Souza, J.J. Queralt, M. Oliva, J. Andrés, Chem. Phys. 264 (2001) 333.
[29] S.A. Brandán, G. Benzal, J.V. García-Ramos, J.C. Otero, A. Ben Altabef, Vib. Spectrosc. 46 (2008) 89–99.
[30] C.E.S. Bernardes, M.F.M. Piedade, M.E. Minas da Piedade, Cryst. Growth Des. 8 (7) (2008) 2419–2430.
[31] P.D. Vaz, P.J.A. Ribeiro-Claro, J. Raman Spectrosc. 34 (2003) 863.